

Self-catalyzed core-shell GaAs/GaNAs nanowires grown on patterned Si (111) by gas-source molecular beam epitaxy

Rui La (刺瑞), , Ren Liu, , Weichuan Yao, , Renjie Chen, , Mattias Jansson, , Janet L. Pan, , Irina A. Buyanova, , Jie Xiang, , Shadi A. Dayeh, and , and Charles W. Tu

Citation: *Appl. Phys. Lett.* **111**, 072106 (2017); doi: 10.1063/1.4990821

View online: <http://dx.doi.org/10.1063/1.4990821>

View Table of Contents: <http://aip.scitation.org/toc/apl/111/7>

Published by the [American Institute of Physics](#)

Articles you may be interested in

[Optically active dilute-antimonide III-nitride nanostructures for optoelectronic devices](#)
Applied Physics Letters **111**, 061101 (2017); 10.1063/1.4997450

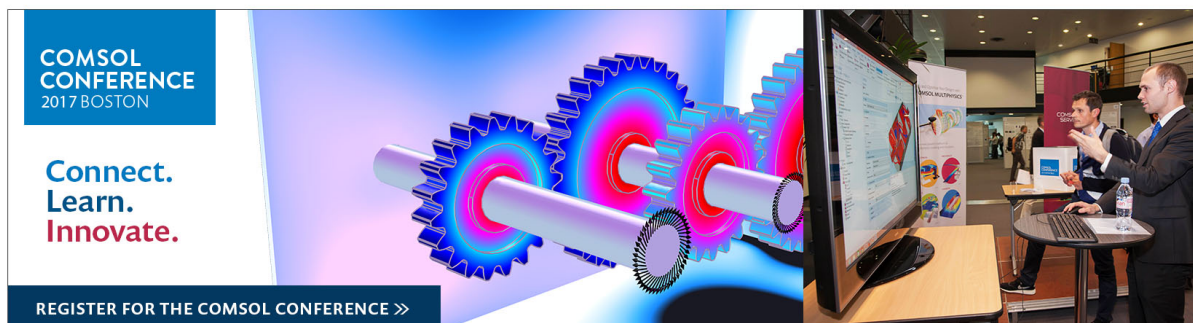
[Terahertz spectroscopy of an electron-hole bilayer system in AlN/GaN/AlN quantum wells](#)
Applied Physics Letters **111**, 073102 (2017); 10.1063/1.4996925

[Chip-scale white flip-chip light-emitting diode containing indium phosphide/zinc selenide quantum dots](#)
Applied Physics Letters **111**, 072104 (2017); 10.1063/1.4999094

[Pulsed laser deposition for the synthesis of monolayer WSe₂](#)
Applied Physics Letters **111**, 073101 (2017); 10.1063/1.4986851

[KF post-deposition treatment of industrial Cu\(In, Ga\)\(S, Se\)₂ thin-film surfaces: Modifying the chemical and electronic structure](#)
Applied Physics Letters **111**, 071601 (2017); 10.1063/1.4998445

[Carrier effects on ferromagnetism of Mn_xGe_{1-x} quantum dots](#)
Applied Physics Letters **111**, 072103 (2017); 10.1063/1.4998933



Self-catalyzed core-shell GaAs/GaNAs nanowires grown on patterned Si (111) by gas-source molecular beam epitaxy

Rui La (刺瑞),¹ Ren Liu,² Weichuan Yao,² Renjie Chen,² Mattias Jansson,³ Janet L. Pan,² Irina A. Buyanova,³ Jie Xiang,^{1,2} Shadi A. Dayeh,^{1,2,4} and Charles W. Tu^{1,2}

¹Graduate Program of Material Science and Engineering, University of California, San Diego, La Jolla, California 92093, USA

²Department of Electrical and Computer Engineering, University of California, San Diego, La Jolla, California 92093, USA

³Department of Physics, Chemistry and Biology, Linköping University, Linköping 58183, Sweden

⁴Department of NanoEngineering, University of California, San Diego, La Jolla, California 92093, USA

(Received 18 June 2017; accepted 6 August 2017; published online 15 August 2017)

We report structural studies on the epitaxial growth of GaAs/GaNAs core-shell nanowires (NWs) on patterned Si (111) substrates by self-catalyzed selective area growth using Gas-Source Molecular Beam Epitaxy. Epitaxial growth conditions were obtained using a combination of dry and time-sensitive wet etching of the SiO₂ growth mask and native SiO₂ layer, respectively. We found that higher growth temperatures resulted in a higher yield for the epitaxial growth of patterned self-catalyzed GaAs NWs on Si with an optimal temperature of 690 °C. The GaNAs shell growth at 500 °C was found to be conformal and maintained an epitaxial and dislocation-free interface with both the Si substrate and the GaAs nanowire. The micro-photoluminescence (μ -PL) measurement at 6 K revealed two bands peaking at 1.45 and 1.17 eV, which could be emission from the GaAs core and GaNAs shell. Transmission electron microscopy showed the zincblende crystal structure of GaAs and GaAs/GaNAs core-shell NWs with minimal twinning near the base of the GaAs nanowires and at the tips of the GaAs/GaNAs core/shell nanowires. This study illustrates the feasibility of the epitaxial growth of patterned GaAs with dilute nitride shells on Si substrates, which would have potential for Si-friendly intermediate band solar cells and telecom emitters. Published by AIP Publishing. [<http://dx.doi.org/10.1063/1.4990821>]

In recent years, III-V semiconductor nanowire (NW) growth on Si substrates has raised considerable interest because it combines the superior physical properties of III-V materials with the standard Si integrated circuits and systems for potential applications in nanophotonic and nanoelectronic devices.^{1–3} One of the advantages for growing III-V NWs on Si substrates as opposed to planar films is that the nanowire geometry effectively relaxes the lattice mismatch constraints due to their small interfacial area.^{4,5} As a result, the interface between the III-V nanowire and the Si substrate can possess minimal interfacial defect densities, low to no antiphase domain boundaries, and under optimized growth conditions defect-free III-V nanowire materials, all of which are attributes that are hard to accomplish with conventional planar thin film growth. Achieving functional devices such as high-efficiency NW solar cells^{6,7} necessitates the growth of NWs at precise positions. Additionally, the parasitic cluster deposition (i.e., inter-nanowire planar growth), which is often accompanied by the NW growth on unpatterned substrates, can be suppressed by patterned growth. Therefore, significant work has been reported on III-V NW growth on patterned Si substrates using the gold-catalyzed method.^{8,9} To avoid contamination associated with foreign metal catalytic droplets including Au, the self-catalyzed growth method, i.e., deposition of one layer of Ga droplets on a Si substrate to seed one dimensional nanowire growth, has been pursued.^{10,11}

Our work focuses on dilute nitride semiconductor layers and nanowires, grown by gas-source molecular beam epitaxy

(MBE), which have two unique characteristics of interest within the spirit of this work. First, according to the band anti-crossing (BAC) model,^{12–14} the interaction between the host states and the N localized states in a dilute nitride system results in two subbands, a lower subband (E₋) that can play the role of an intermediate band (IB) and a higher subband (E₊) that plays the role of the conduction band (CB). Electrons can be excited from the valence band (VB) to the CB via the IB through two-photon absorption, which makes the dilute nitride materials of great importance for the fundamental study of light-matter interactions and of special interest for the field of solar cell research.^{15,16} Second, the giant bowing in the bandgap energy of III-N-V alloys makes them technologically attractive for long-wavelength lasers within the optical-fiber communication wavelength window (1.3–1.55 μ m).^{17,18} To improve the carrier lifetime, the suppression of the surface states by growing a shell layer of AlGaAs or GaAsP is of crucial importance. However, the opposite trend was recently reported¹⁹ for GaNAs NWs, the room-temperature carrier lifetime of which was found to be improved. The reason could be the formation of Ga-N bonds at the GaAs surface, which causes the passivation of Ga dangling bonds.²⁰ Hence, we investigated GaAs/GaNAs core/shell NWs.

The self-catalyzed growth of GaAs/GaNAs nanowires on Si (111) has been pursued before by several groups. While fundamental studies^{21–23} have advanced our understanding of the carrier dynamics in GaAs/GaNAs core/shell nanowires, the patterned growth of GaAs/GaNAs core/shell

nanowires—important for device applications—has not been attempted. Further, detailed and high resolution transmission electron microscopy (HRTEM) studies to uncover the quality of the GaAs/Si and GaAs/GaNAs/Si interfaces are yet to be performed. This work presents mechanistic studies to enable the controlled growth of GaAs/GaNAs core/shell nanowires in precisely defined patterns using the selective area growth approach, optical characterization, and the HRTEM study of the interfacial and structural characteristics of the grown layers.

We utilize standard electron beam lithography (EBL)²⁴ and $\text{CF}_4/\text{CHF}_3/\text{Ar}$ anisotropic dry etching of 30 nm-thick plasma enhanced chemical vapor deposited (PECVD) SiO_2 growth mask layers on Si (111) substrates. The patterned array consisted of holes with a diameter of ~ 90 nm and an inter-hole center spacing (pitch) of $1.5 \mu\text{m}$. Prior to the introduction of the samples into the MBE chamber, a short diluted aqueous hydrofluoric acid (HF) dip was used in order to etch the native oxide from the patterned holes. The growth was performed in a Varian Gen-II MBE system modified to handle gas sources. Thermally cracked AsH_3 was used as the As_2 source, while solid elemental Ga was used to generate a Ga atomic beam through an effusion cell. The substrate was heated to 690°C for 15 min prior to the growth.

For NW growth, Ga was deposited on the Si (111) surface for 1 min with a Ga flux of ~ 0.7 monolayer/s, calibrated by Ga-induced reflection high-energy electron diffraction (RHEED) intensity oscillation for the planar homoepitaxial growth of GaAs at the same substrate temperature (T_{sub}). As incorporation was also determined from As-induced RHEED intensity oscillation on a Ga-rich surface.²⁵ Then, the substrate was annealed for 30 s to form Ga droplets inside the holes. The GaAs NWs were grown for 20 min at a V/III incorporation ratio of 2 and a substrate rotation speed of 3 RPM for growth uniformity. The AsH_3 flow rate was set at 3 sccm during growth. Scanning electron microscopy (SEM) measurements of the NWs were performed with an FEI XL30 ultra high resolution SEM system.

We first investigated the effect of using a diluted HF solution to remove the native oxide in the patterned holes prior to the growth of GaAs NWs. Figure 1 shows 45° -tilted SEM images of GaAs NWs with various diluted HF etching times. These results suggest that (1) the patterned holes in Fig. 1(a)—no HF etching—are completely covered by SiO_2 ; (2) holes for the 10 s HF etching [Fig. 1(b)] are partly covered by SiO_2 prior to NW growth; (3) holes for the 30 s HF etching [Fig. 1(c)] have their native oxide properly etched and were properly filled with Ga droplets for GaAs NW growth; and (4) holes for the 60 s HF etching [Fig. 1(d)] are fully etched together with the formation of etch-pits in SiO_2 in EBL non-patterned regions due to the damage of the SiO_2 pattern in the long HF dip, leading to Ga accumulation in the parasitic NW growth. Therefore, we conclude that a 30 s HF dip is optimal for selective area GaAs NW growth under our otherwise fixed experimental conditions.

Next, we optimized the morphology of the grown GaAs NWs by studying the effects of the growth temperatures, T_{sub} , of 630, 650, 670, and 690°C . Prior to growth, all the samples were dipped in diluted HF for 30 s to fully remove the native oxide. We find that the higher the growth

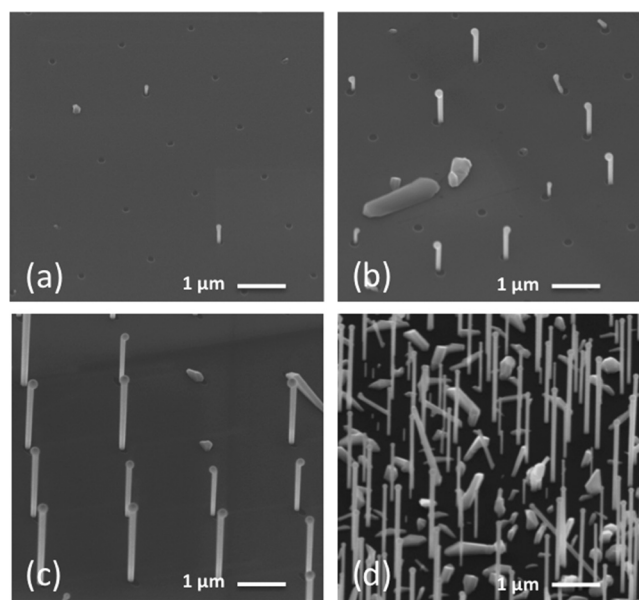


FIG. 1. SEM images of GaAs core NWs on Si (111) with diluted HF etching times of (a) $t = 0$ s, (b) $t = 10$ s (c) $t = 30$ s, and (d) $t = 60$ s. The Ga flux was set at 0.7 monolayer/s, and growth time = 20 min. HF was diluted in DI water at a ratio of 1:40.

temperature, the higher the NW growth yield. In the vapor-liquid-solid (VLS) mechanism,²⁶ liquid droplets act as a catalyst and absorb vapor components (both Ga and As here) to get incorporated into and supersaturate alloy droplets (Ga rich here) and initiate the growth of the reaction byproduct (GaAs NW) from a supersaturated melt. At sufficiently high T_{sub} ($\geq 650^\circ\text{C}$), the Ga adatom mobility is increased. Consequently, most adatoms can diffuse into the Ga droplet in the SiO_2 hole or on the NW tip, which provides abundant Ga replenishment for a well-supersaturated GaAs NW VLS growth.

With the optimization of the GaAs NW core growth, we proceeded to the dilute nitride shell growth, which permits the growth of advanced structures by doping and composition modulation, such as p-i-n radial junctions and heterojunctions including quantum wells. For GaAs/GaNAs core/shell NWs, T_{sub} for the shell growth was decreased to $\sim 500^\circ\text{C}$. Decreasing T_{sub} reduces the Ga adatom mobility on the growing surfaces and depletes the NW tip from a liquid Ga droplet to cease the axial NW growth. However, the Ga shutter was closed while ramping down the growth temperature for 20 min and keeping the group V flux to consume the Ga droplets prior to the growth of the GaNAs shells. The Ga flux is kept at 0.7 monolayer/s. The N plasma power conditions for the shell were 0.9 sccm and 250 W, and the shell growth time was 30 min. Figure 2(a) shows the SEM image of the core-shell GaAs/GaNAs NWs. The average diameter of core-shell NWs is ~ 220 nm. The μ -PL measurement was carried out on as-grown NW arrays with excitation from a 659 nm solid-state laser source at 6 K. The excitation beam was focused on the sample using a $50\times$ objective (NA = 0.5). The excitation power was 1 mW. The signal was dispersed using a monochromator equipped with a 950 mm^{-1} grating and detected with a liquid nitrogen cooled InGaAs CCD. Figure 2(b) shows the μ -PL measurement of the core-shell NWs (the solid line) together with the reference GaAs

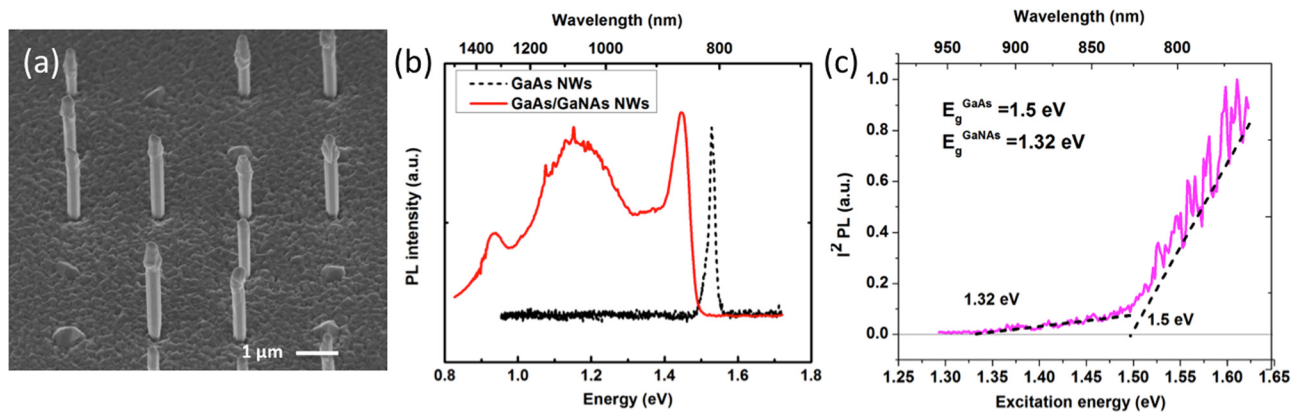


FIG. 2. (a) SEM images of GaAs/GaNAs core-shell NWs. (b) μ -PL spectra of the GaAs NWs and GaAs/GaNAs NWs measured under 659 nm excitation. (c) PLE spectrum detected from the GaAs/GaNAs core-shell NWs, plotted as the square of the PL-intensity (I_{PL}).

NWs (the dashed line). The spot diameter of the μ -PL laser beam focused on the sample is estimated to be 0.8–1 μ m, which means that the PL-spectra came from one or two NWs. The μ -PL spectrum of the reference sample is dominated by a single line at around 1.52 eV, likely due to free exciton (FE) recombination. The lack of other transitions in the spectra indicates very good structural and optical quality of the sample, consistent with the results of TEM measurements to be discussed below. For the GaAs/GaNAs core-shell NWs, the PL spectra contain two dominant emission bands peaking at 1.45 and 1.17 eV. The former could be attributed to the GaAs core based on performed photoluminescence excitation (PLE) measurements [Fig. 2(c)]. We note that the GaAs emission in the core-shell structures is no longer dominated by the FE transitions, which could reflect fast FE trapping by the shell with a lower bandgap. Instead, it contains a broader PL band, which likely arises from radiative transitions involving residual impurities or defects formed due to the strain in the core-shell structure. The second PL band is due to emission from the GaNAs shell and arises from the recombination of weakly localized excitons, which are trapped by potential fluctuations induced by long-range alloy disorder in the GaNAs shell.¹⁹ The numerous fine features overlapping with the broad peak could be attributed to excitons strongly confined in quantum-dot like states induced by short-range fluctuations in the nitrogen composition which are superimposed on long-range alloy disorder.²⁷ The third peak at around 0.93 eV may be caused by N related defects, which is often seen in dilute nitride materials.^{22,28} The N composition is estimated to be \sim 0.8% using the band anti-crossing (BAC) model and PLE spectra detected from GaAs/GaNAs core-shell NWs in Fig. 2(c).

We then studied the interface of the selective area grown GaAs NW and GaAs/GaNAs core/shell NWs with the Si substrate using TEM. To prepare the samples for TEM, we first deposited a 200 nm-thick SiO₂ layer by PECVD and then deposited a Pt protection layer by *in-situ* focused ion beam (FIB). Second, careful FIB slicing at the GaAs NW growth site from the Si substrate was performed. The sample was then mounted by a controlled manipulator inside the FIB on a TEM grid and was further thinned to an e-beam transparent lamella thickness in the range of 80–120 nm. An overall view of the studied GaAs NW is shown in Fig. 3(a)

where the NW grows from the SiO₂ hole and increases the diameter above the hole to overlap its edge. Overall, we found that the GaAs NW grown on the Si substrate at 690 °C exhibited the zincblende crystal structure [Figs. 3(b)–3(d), 3(f)] and was relatively free of defects except for a few twinning planes observed in the hole and near the base of the NW. These twinning planes are commonly observed for III-V semiconductor NWs due to the small energy difference between the zincblende (ZB) phase and the hexagonal wurtzite (WZ) phase.²⁹ In addition to the free NW surface that helps in stress relief, the stepped morphology of the GaAs NW at the SiO₂ mask at the base is expected to significantly lower the strain near the base of the GaAs nanowire, thereby minimizing the formation of edge dislocations and twin boundaries at the GaAs/Si heterointerface [Fig. 3(d)].³⁰ On a stepped interface, there are atoms at the edges that can be dislocated from their pre-supposed position on a flat interface. These atoms at multiple edges can adapt to strain, and the interfacial in-plane strain is supposed to be reduced and be accommodated. The strain distribution was calculated by manually measuring atomic distances at different locations near the Si/GaAs interface in Fig. 3(d). According to the strain distribution analysis in Fig. 3(e), the in-plane strain (ϵ_{\parallel}) in the Si substrate at 1.2 nm from the interface is 1.3%, and the in-plane strain (ϵ_{\parallel}) in the GaAs core at 1.2 nm from the interface is -1.7%. The in-plane strain (ϵ_{\parallel}) and out-of-plane strain (ϵ_{\perp}) in Si decrease gradually to nearly 0 at 12 nm from the interface. Of note is the stepped diameter before, at, and after the planar twinned layer near the base as shown in Fig. 3(f). Recent *in-situ* TEM growth of GaAs NWs concludes that their phase is dictated by the dynamics of the catalyst volume and contact angle at the edge of the NW.³¹ The change in the Ga droplet volume during the growth affects the phase of the crystal and consequently the diameter of NWs.

It is imperative to study the interfaces of the GaNAs shells on GaAs NWs. Figure 4(a) shows an overall TEM image view of a GaAs/GaNAs core-shell NW grown on the Si substrate. Defective growth at the tip of the NW is observed in Fig. 4(b), indicating that the Ga droplet was not fully depleted prior to the GaNAs shell growth. The magnified image of the NW base in Fig. 4(c) reveals that the parasitic GaNAs is grown on the SiO₂ pattern at a substrate

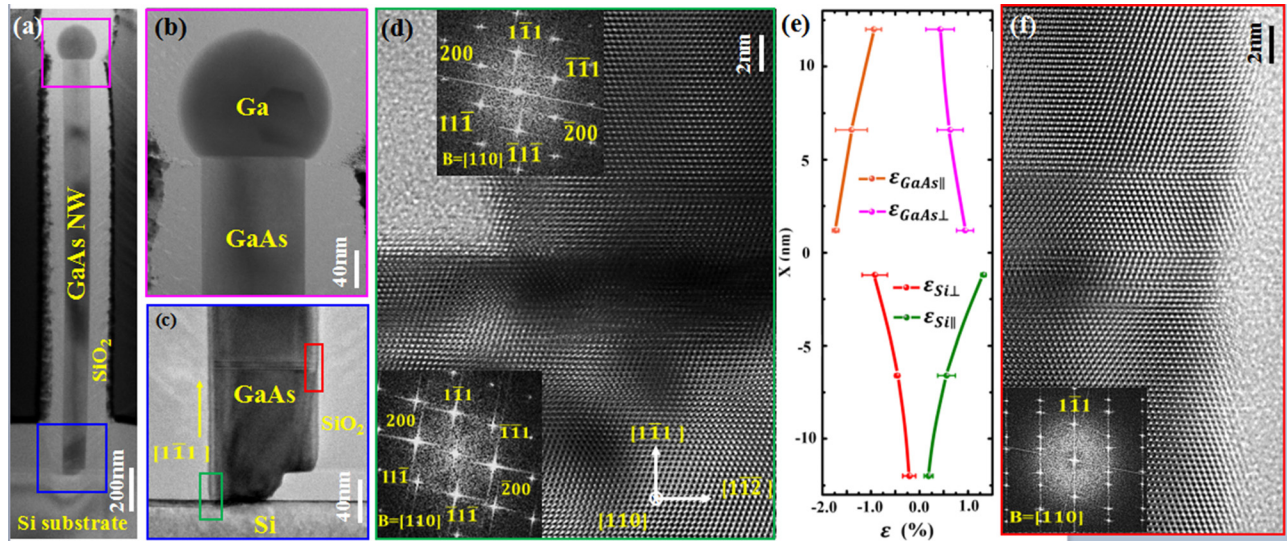


FIG. 3. (a) TEM image of an overview of a GaAs NW on a Si substrate. (b) High-magnification TEM image of the tip of the GaAs NW. (c) High-magnification TEM image of the bottom of the GaAs NW on the Si substrate. (d) High-resolution TEM (HRTEM) image of the interface of the GaAs NW and Si substrate indicated by the green rectangle in (c). (e) The strain distribution at the interface of the GaAs NW and Si substrate. (f) HRTEM image of a part of the NW near the base indicated by the red rectangle in (c) showing the twinning planes in the GaAs NW. The insets in (d) and (f) show the Fast Fourier Transform (FFT) of the crystal in respective regions.

temperature of $\sim 500^\circ\text{C}$ with a thickness of ~ 200 nm. The catalyzed growth on the SiO₂ surface is about 4 times thicker than that on the NW sidewalls, which was ~ 55 nm. The strain between GaAs and GaNAs on the sidewall was estimated to be $\sim 0.18\%$ for an expected nitrogen concentration of 0.8% in these experiments.³² Using the Matthews and Blakeslee force balance for strain relaxation, the critical thickness of planar GaNAs containing 0.8% nitrogen on GaAs was calculated to be ~ 180 nm.³³ Core/shell nanowires are known to have a larger critical thickness for strain

relaxation compared to planar layers.³⁴ Thus, the boundary between GaAs and GaNAs is not obvious in the TEM image. Interestingly, we found that GaNAs filled laterally the empty space in the patterned hole and epitaxially grew on the Si (111) surface as observed in Figs. 4(d)–4(g). The HRTEM images at the Si/GaNAs interface did not reveal evident defects except for the planar twinned layers within the GaAs/GaNAs core/shell NW. We suspect that these planar defects also help in relieving the $\sim 4\%$ GaAs/Si lattice mismatch, in addition to the free surface. Future work will

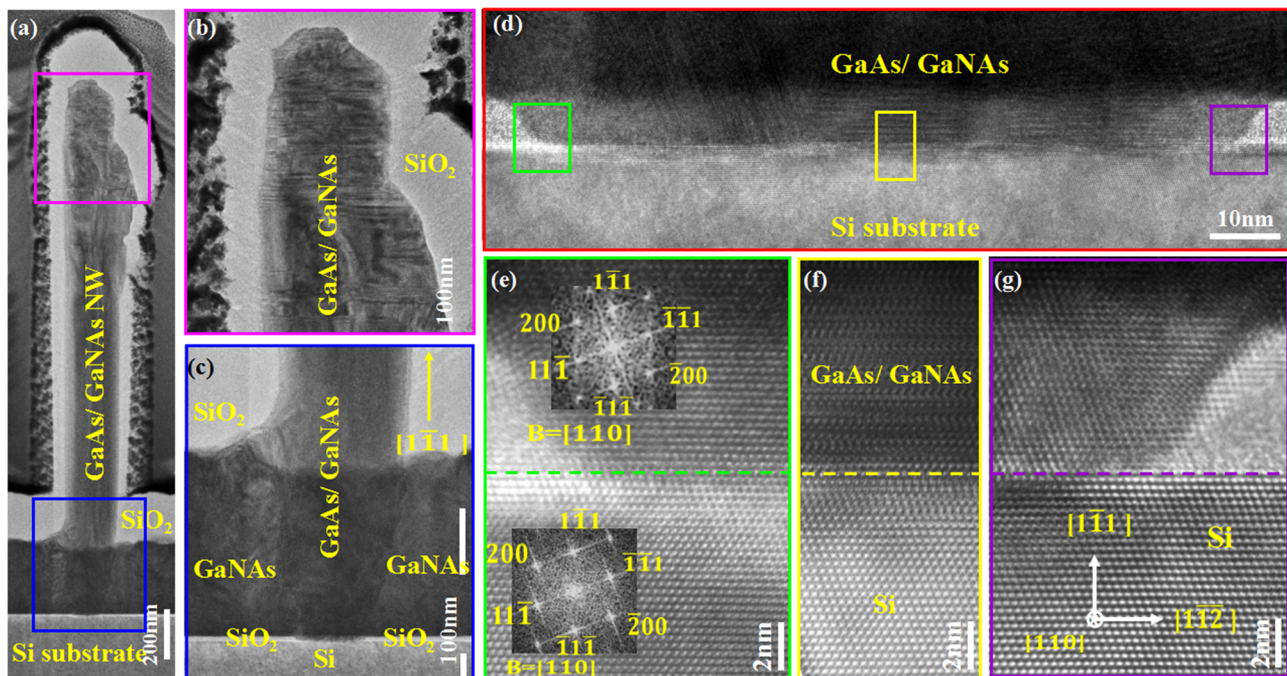


FIG. 4. (a) TEM image of an overview of a GaAs/GaNAs core-shell NW on a Si substrate. (b) High-magnification TEM image of the tip of the GaAs/GaNAs core-shell NW. (c) High-magnification TEM image of the bottom of the GaAs/GaNAs core-shell NW on the Si substrate. (d) HRTEM image of the interface of the GaAs/GaNAs NW and Si substrate. (e)–(g) HRTEM images of the interface of the GaAs/GaNAs NW and Si, respectively (green, yellow, and purple rectangles in (d)). The inset in (e) and (g) shows the selected-area diffraction pattern.

concern with the optimization of the shell growth conditions and Ga depletion from the NW tip to enable an epitaxial defect-free core/shell tip that is crucial for light absorption or emission.

In summary, vertical self-catalyzed GaAs NWs and GaAs/GaNAs core-shell NWs were grown on patterned Si (111) substrates by Gas-Source Molecular Beam Epitaxy (GSMBE). The typical diameters are ~ 110 nm for GaAs NWs and ~ 220 nm for GaAs/GaNAs core-shell NWs for a shell growth time of 30 min. The yield of vertical NW growth increased by optimal wet etching of the native oxide layers and at higher growth temperatures with the best result obtained at 690 °C. GaNAs shells were grown and maintained an epitaxial interface with both the Si substrate and the GaAs NW core deduced from detailed HRTEM studies.

This work was performed in part at the San Diego Nanotechnology Infrastructure (SDNI) of UCSD, a member of the National Nanotechnology Coordinated Infrastructure, which is supported by the National Science Foundation (Grant No. ECCS-1542148). The TEM work was performed at the Center for Integrated Nanotechnologies (CINT), U.S. Department of Energy, Office of Basic Energy Sciences User Facility at Los Alamos National Laboratory (Contract No. DE-AC52-06NA25396) and Sandia National Laboratories (Contract No. DE-AC04-94AL85000). Optical characterization at Linköping University was supported in part by the Swedish Energy Agency (Grant No. P40119-1) and the Swedish Research Council (Grant No. 2015-05532).

- ¹Y. J. Kuang, S. Sukrittanon, H. Li, and C. W. Tu, *Appl. Phys. Lett.* **100**, 053108 (2012).
- ²M. S. Gudiksen, L. J. Lauhon, D. Wang, C. Smith, and C. M. Lieber, *Nature* **415**, 617 (2002).
- ³S. A. Dayeh, C. Soci, X. Bao, and D. Wang, *Nano Today* **4**, 347 (2009).
- ⁴F. Glas, *Phys. Rev. B* **74**, 121302 (2006).
- ⁵L. C. Chuang, M. Moewe, C. Chase, N. P. Kobayashi, C. Chang-Hasnain, and S. Crankshaw, *Appl. Phys. Lett.* **90**, 043115 (2007).
- ⁶M. Yao, N. Huang, S. Cong, C. Chi, M. A. Seyed, Y. Lin, Y. Cao, M. L. Povinelli, P. D. Dapkus, and C. Zhou, *Nano Lett.* **14**, 3293 (2014).
- ⁷J. Wallentin, N. Anttu, D. Asoli, M. Huffman, I. Aberg, M. H. Magnusson, G. Siefert, P. Fuss-Kailuweit, F. Dimroth, B. Witzigmann, H. Q. Xu, L. Samuelson, K. Deppert, and M. T. Borgstrom, *Science* **339**, 1057 (2013).

- ⁸K. Tomioka, P. Mohan, J. Noborisaka, S. Hara, J. Motohisa, and T. Fukui, *J. Cryst. Growth* **298**, 644 (2007).
- ⁹E. Nakai, M. Yoshimura, K. Tomioka, and T. Fukui, *Jpn. J. Appl. Phys., Part 1* **52**, 055002 (2013).
- ¹⁰M. Bar-Sadan, J. Barthel, H. Shtrikman, and L. Houben, *Nano Lett.* **12**, 2352 (2012).
- ¹¹Y. Wang, V. Schmid, S. Senz, and U. Gosele, *Nat. Nanotechnol.* **1**, 186 (2006).
- ¹²H. P. Xin, C. W. Tu, Y. Zhang, and A. Mascarenhas, *Appl. Phys. Lett.* **76**, 1267 (2000).
- ¹³W. Shan, W. Walukiewicz, J. W. Ager III, E. E. Haller, J. F. Geisz, D. J. Friedman, J. M. Olson, and S. R. Kurtz, *Phys. Rev. Lett.* **82**, 1221 (1999).
- ¹⁴J. Wu, W. Shan, and W. Walukiewicz, *Semicond. Sci. Technol.* **17**, 860 (2002).
- ¹⁵R. Kudrawiec, A. V. Luce, M. Gladysiewicz, M. Ting, Y. J. Kuang, C. W. Tu, O. D. Dubon, K. M. Yu, and W. Walukiewicz, *Phys. Rev. Appl.* **1**, 034007 (2014).
- ¹⁶A. Luque, A. Marti, and C. Stanley, *Nat. Photonics* **6**, 146 (2012).
- ¹⁷M. Kondow, K. Uomi, A. Niwa, T. Kitatani, S. Watahiki, and Y. Yazawa, *Jpn. J. Appl. Phys., Part 1* **35**, 1273 (1996).
- ¹⁸W. G. Bi, Y. Ma, J. P. Zhang, L. W. Wang, S. T. Ho, and C. W. Tu, *Photonics Technol. Lett.* **9**, 1072 (1997).
- ¹⁹S. L. Chen, S. Filippov, F. Ishikawa, W. M. Chen, and I. A. Buyanova, *Appl. Phys. Lett.* **105**, 253106 (2014).
- ²⁰S. L. Chen, W. M. Chen, F. Ishikawa, and I. A. Buyanova, *Sci. Rep.* **5**, 11653 (2015).
- ²¹Y. Araki, M. Yamaguchi, and F. Ishikawa, *Nanotechnology* **24**, 065601 (2013).
- ²²J. E. Stehr, S. L. Chen, M. Jansson, F. Ishikawa, W. M. Chen, and I. A. Buyanova, *Appl. Phys. Lett.* **109**, 203103 (2016).
- ²³S. Chen, M. Jansson, S. Filippov, F. Ishikawa, W. M. Chen, and I. A. Buyanova, *J. Vac. Sci. Technol. B* **34**, 04J104 (2016).
- ²⁴S. Plissard, G. Larrieu, X. Wallart, and P. Caroff, *Nanotechnology* **22**, 275602 (2011).
- ²⁵T. P. Chin, B. W. Liang, H. Q. Hou, M. C. Ho, C. E. Chang, and C. W. Tu, *Appl. Phys. Lett.* **58**, 254 (1991).
- ²⁶R. S. Wagner and W. C. Ellis, *Appl. Phys. Lett.* **4**, 89 (1964).
- ²⁷S. Filippov, M. Jansson, J. E. Stehr, J. Palisaitis, P. O. A. Persson, F. Ishikawa, W. M. Chen, and I. A. Buyanova, *Nanoscale* **8**, 15939 (2016).
- ²⁸Y. J. Kuang, S. Chen, H. Li, S. K. Sinha, and C. W. Tu, *J. Vac. Sci. Technol., B* **30**, 02B121 (2012).
- ²⁹S. Sukrittanon, Y. J. Kuang, and C. W. Tu, *J. Vac. Sci. Technol., B* **31**, 03C110 (2013).
- ³⁰R. Chen and S. A. Dayeh, *Nano Lett.* **15**, 3770 (2015).
- ³¹D. Jacobsson, F. Panciera, J. Tersoff, M. C. Reuter, S. Lehmann, S. Hofmann, K. A. Dick, and F. M. Ross, *Nature* **531**, 317 (2016).
- ³²W. Li and M. Pessa, *Appl. Phys. Lett.* **78**, 2864 (2001).
- ³³J. W. Matthews and A. E. Blakeslee, *J. Cryst. Growth* **27**, 118 (1974).
- ³⁴S. A. Dayeh, W. Tang, F. Boioli, K. L. Kavanagh, H. Zheng, J. Wang, N. H. Mack, G. Swadener, J. Y. Huang, L. Miglio, K. N. Tu, and S. T. Picraux, *Nano Lett.* **13**, 1869 (2013).